Journal of Crystal Growth 363 (2013) 205–210

Contents lists available at SciVerse ScienceDirect

Journal of Crystal Growth

journal homepage: www.elsevier.com/locate/jcrysgro

Pseudomorphic growth and strain relaxation of α-Zn_3P_2 on GaAs(001) by molecular beam epitaxy

Jeffrey P. Bosco*, Gregory M. Kimball, Nathan S. Lewis, Harry A. Atwater

Watson Laboratory and Noyes Laboratory, California Institute of Technology, 1200 East California Boulevard, Pasadena, CA 91125, USA

ARTICLE INFO

Article history:
Received 10 January 2012
Received in revised form
6 September 2012
Accepted 21 October 2012
Communicated by A. Brown
Available online 3 November 2012

Keywords:
A1. Pseudomorphic growth
A1. X-ray diffraction
A3. Molecular beam epitaxy
B1. Phosphides
B3. Solar cells

ABSTRACT

Tetragonal zinc phosphide (α-Zn_3P_2) was grown pseudomorphically, by compound-source molecular-beam epitaxy on GaAs(001). The films grew coherently strained, with epitaxial relationships of Zn_3P_2(004)‖GaAs(002) and Zn_3P_2(202)‖GaAs(1$\bar{1}$1). Partial relaxation of the Zn_3P_2 lattice was observed for films that were >150 nm in thickness. Van der Pauw and Hall effect measurements indicated that the films were intrinsically p-type, presumably due to the incorporation of phosphorus interstitials. The carrier mobilities in strained films (>40 cm^2 V^{-1} s^{-1}) were comparable to the carrier mobilities that have been reported for bulk Zn_3P_2 single crystals. The carrier densities and mobilities of holes decreased significantly upon film relaxation, consistent with the evolution of compensating dislocations.

1. Introduction

Terawatt-scale photovoltaics (PV) will require a low-cost, earth-abundant semiconductor material that has excellent optoelectronic properties. Zn_3P_2 is an interesting, potentially efficient, solar absorber, with a near optimal, direct band gap of 1.50 eV and with a high visible-light absorption coefficient ($>10^4$ cm^{-1}) near the band edge [1–4]. Furthermore, Zn_3P_2 has been reported to have long (>5 μm) minority-carrier diffusion lengths [5,6] as well as passive grain boundaries [7]. These properties, in addition to the abundance and low cost of elemental zinc and phosphorus, make Zn_3P_2 attractive for scalable thin-film applications. Studies of Zn_3P_2 as a PV material have primarily focused on the properties of multicrystalline wafers and/or polycrystalline films, with reported maximum solar energy-conversion efficiencies of 6.0% and 4.3%, respectively [6,8]. In contrast, the growth of, and properties of, epitaxial Zn_3P_2 thin films is less well-understood. Dislocation free, single crystalline films will likely result in improved device performance and ultimately in higher PV efficiencies.

Zn_3P_2 epitaxy has been reported by Suda et al. on GaAs(001) and ZnSe(001) substrates through the use of metal-organic chemical-vapor deposition (MOCVD) as well as by molecular-beam epitaxy (MBE) with elemental sources [9,10]. GaAs and ZnSe substrates were used because these materials have a relatively small lattice mismatch with the phosphorus sublattice in the tetragonal α-Zn_3P_2 unit cell (1.3% and 1.0%, respectively). The epitaxial layers grew along the Zn_3P_2(001) crystallographic orientation, independent of the substrate material. However, reflection high-energy electron diffraction (RHEED) patterns showed that the growths were three-dimensional in nature. Liquid-phase epitaxy of Zn_3P_2 on InP(001) has also been reported [11]. Using molten In as the solvent, oriented growth was achieved through control of the cooling rate of the solvent. These films were polycrystalline and had very high hole carrier concentrations ($>10^{18}$ cm^{-3}), consistent with the unintentional incorporation of In as an extrinsic p-type dopant.

We report herein the growth of Zn_3P_2 epitaxial layers on GaAs(001) substrates by compound-source MBE. A compound source is possible because Zn_3P_2 sublimes congruently according to the following dissociation reaction [12]:

$$Zn_3P_2\ (s) \rightarrow 3Zn\ (g) + \frac{1}{2}P_4\ (g) \quad (1)$$

This behavior allows a simple and controllable approach to achieve stoichiometric beam fluxes of zinc and phosphorus. Previous studies of Zn_3P_2 films grown from a compound source have focused on close-space sublimation (CSS) and hot-wall deposition (HWD) techniques. CSS has been used to deposit large-grained (1–10 μm), photovoltaically active, polycrystalline Zn_3P_2 films on Si/Fe-coated mica substrates [8]. On freshly cleaved KCl(001) or on mica substrates, HWD has been used to produce Zn_3P_2 polycrystalline films that had partial orientation toward the (224) direction [13]. On GaAs(001) and borosilicate

* Corresponding author. Tel.: +1 626 395 3330; fax: +1 626 844 9320.
E-mail address: jbosco@caltech.edu (J.P. Bosco).

0022-0248/$ - see front matter © 2012 Elsevier B.V. All rights reserved.
http://dx.doi.org/10.1016/j.jcrysgro.2012.10.054

glass substrates, the HWD technique has also been used to produce strongly preferred orientation of polycrystalline Zn_3P_2 films toward the (004) direction, and in-plane texturing [14,15]. Our work builds upon previous Zn_3P_2 thin film growth studies and demonstrates the formation of single-crystalline, coherently strained, Zn_3P_2 epitaxial layers.

2. Experimental details

Zn_3P_2 films were grown in an ultra-high vacuum MBE chamber that had an ultimate pressure of $<2\times10^{-10}$ Torr. The Zn_3P_2 source material was synthesized from elemental zinc and phosphorus (99.9999%, Alfa Aesar) at 850 °C [16–18]. A standard Knudsen effusion cell was used to provide the compound sublimation source. Epi-ready, semi-insulating GaAs(001) single crystal wafers (AXT) were used as epitaxial substrates. The GaAs was mounted to a Mo chuck using an In–Ga eutectic. The substrate was degassed at 350 °C for 1 h in vacuum, and the native oxide was removed by exposure at 450 °C to an atomic hydrogen flux for ~30–40 min [19–22]. The removal of the native oxide was verified in situ using RHEED, which yielded a streaky (1×1) surface reconstruction. Removal of the GaAs native oxide by annealing the substrate at >580 °C for 20 min also enabled the growth of epitaxial Zn_3P_2. However, this method of substrate preparation resulted in large pits in the GaAs surface, and therefore decreased the quality of the subsequent epilayer growth. Complete removal of the GaAs native oxide was required to obtain pseudomorphic Zn_3P_2 film growth. The presence of a uniform oxide layer consistently resulted in the deposition of amorphous Zn_3P_2, independent of the growth conditions employed. In contrast, incomplete removal of the GaAs oxide led to polycrystalline film growth because columnar grains of crystalline Zn_3P_2 were seeded by the GaAs substrate through pinholes in the amorphous oxide layer.

To determine the optimal MBE growth window, Zn_3P_2 films were initially grown at substrate temperatures between 150 °C and 300 °C. In-situ RHEED was used to monitor the initial and final stages of the growth process. Once suitable conditions for epitaxial growth were determined, the morphological, crystallographic, and optoelectronic properties of Zn_3P_2 epilayers of varying thicknesses were investigated using a number of ex-situ techniques, including atomic force microscopy (AFM), high-resolution X-ray diffraction (HRXRD), transmission electron microscopy (TEM), spectroscopic ellipsometry, and Van der Pauw and Hall effect measurements, allowing for a direct comparison between the electrical properties of strained and relaxed Zn_3P_2 films.

3. Results and discussion

Fig. 1 displays the growth rate of Zn_3P_2 as a function of the substrate temperature, for a BEP of $\sim1\times10^{-6}$ Torr. For substrate temperatures <250 °C, the growth rate was typically 3–4 nm min^{-1}. For temperatures >250 °C, a rapid decline in the growth rate was observed, consistent with a decrease in the Zn sticking coefficient with increasing temperature. Analogous trends in growth rate have been reported for Zn-containing II–VI compounds, such as ZnSe [23] and ZnS [24]. For comparison, under similar conditions, the growth rate of ZnS produced by compound-source MBE is plotted along with the Zn_3P_2 data. The Zn_3P_2 growth rate decreased over a much narrower temperature range than has been reported for growth of ZnS, with the Zn_3P_2 growth completely terminated by 300 °C. This behavior is expected, because at the temperature range of interest, Zn_3P_2 exhibits a much higher sublimation pressure than ZnS. To allow

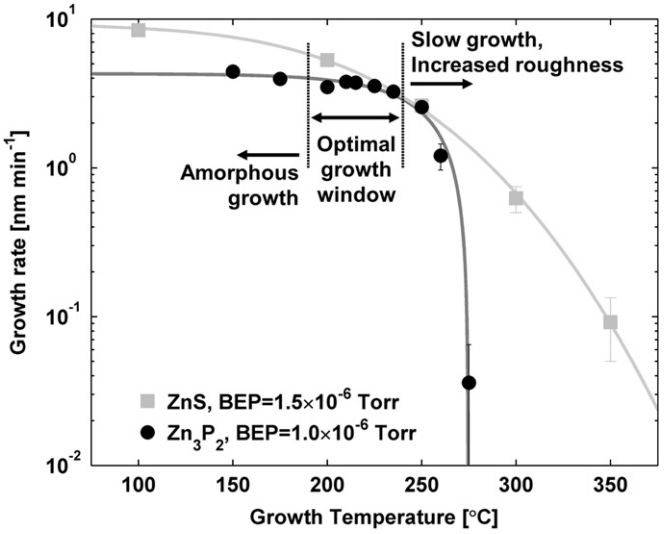

Fig. 1. The growth rate of Zn_3P_2 as a function of substrate temperature for a given BEP of $\sim1\times10^{-6}$ Torr. The growth rate data for ZnS [24] is displayed for comparison. The optimal growth window for Zn_3P_2 epitaxy was between 200 °C and 250 °C.

for Zn_3P_2 epitaxy, the observed rapid reduction in growth rate establishes a practical upper bound of ~250 °C on the substrate temperature.

Fig. 2(a)–(c) displays RHEED images collected along the [100] zone axis of Zn_3P_2 films that were grown at 150 °C, 200 °C, and 250 °C, respectively. The RHEED images of Zn_3P_2 films that were grown at 200–235 °C exhibited streaky (1×1) patterns (Fig. 2(b)), indicating highly crystalline, oriented film growth that occurred two-dimensionally. The faint appearance of half-order streaks in the RHEED patterns suggested that a partial surface reconstruction occurred for thicker films. The reconstruction is consistent with Zn-termination of the Zn_3P_2(001) surface. All RHEED images observed for films that were grown at substrate temperatures ≤175 °C revealed cloudy, specular-beam reflections with only a faint appearance of crystalline peaks, indicating that the films were primarily amorphous (Fig. 2(a)). The amorphous nature of these films was confirmed by XRD. The deposition of amorphous material established a practical lower bound of ~200 °C on the substrate temperature for Zn_3P_2 epitaxy. Spotty RHEED patterns were observed for films that were grown at substrate temperatures of ≥250 °C (Fig. 2(c)), indicating that these films were crystalline and oriented, but that their surfaces were significantly rougher than the surfaces of films that were grown at lower temperatures. The observed increase in roughness is consistent with the partial re-sublimation of the deposited Zn_3P_2 film.

The surface roughness of the as-grown films was verified by AFM topography (Fig. 2(d)–(f)). Films that were grown between 200 and 235 °C had a typical RMS surface roughness of 0.6 nm, whereas films that were grown at ≤175 °C or at ≥250 °C were significantly rougher, having typical RMS roughness values of 2 nm and 10 nm, respectively. The AFM topography results, in addition to the growth rate and RHEED images, indicated that the growth of smooth, epitaxial Zn_3P_2 films was constrained to a narrow temperature window, specifically between 200 °C and 235 °C. To maximize the growth rate and to minimize the surface roughness, all subsequent growths were therefore performed at a substrate temperature of 200 °C.

The RHEED data collected on epitaxial Zn_3P_2 films grown at 200 °C indicated that the Zn_3P_2 tetragonal lattice grew along the (001) direction at a 45° in-plane rotation with respect to the GaAs zinc-blende lattice. Hence, the epitaxial relationship between the

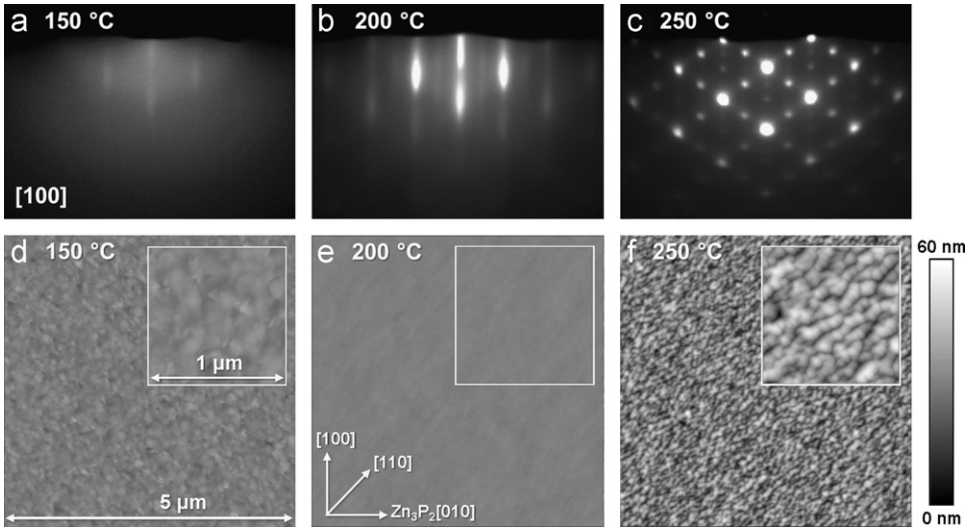

Fig. 2. (a)–(c) In situ RHEED images and (d)–(e) AFM topography images of the Zn_3P_2 surface for films grown at substrate temperatures of 150 °C, 200 °C, and 250 °C, respectively. All of the RHEED images were collected at 20 keV along the GaAs[0$\underline{1}$1] azimuth, corresponding to the Zn_3P_2[100] azimuth for crystalline films. The height scale bar applies to all of the AFM images.

epilayer and the substrate was $Zn_3P_2(004)\|GaAs(002)$ and $Zn_3P_2(202)\|GaAs(1\underline{1}1)$. Selected-area electron diffraction (SAED) of the Zn_3P_2/GaAs interface (inset, Fig. 3(a)), and high-resolution TEM (inset, Fig. 3(b)), confirmed this relationship. Fig. 3(a) and (b) displays bright-field TEM images of the 50 and the 150 nm thick Zn_3P_2 epilayers, respectively. The 50 nm epilayer was effectively dislocation-free, whereas a low concentration of crystalline defects was observed for the 150 nm thick film, indicating the onset of strain relaxation.

Fig. 4(a) displays the symmetric HRXRD of the GaAs(004) and Zn_3P_2(008) reflections that were observed for increasing epilayer thicknesses. Clear Pendellösung oscillations were observed for film thicknesses of <150 nm, indicating highly crystalline thin films. Table 1 reports the 2θ values of the Zn_3P_2(008) peak maximum for all films. A shift in the Zn_3P_2(008) peak position with respect to the bulk 2θ position [25] was observed for film thicknesses up to $\sim$150 nm. This shift represents an out-of-plane strain ($\varepsilon_\perp$) value of approximately 0.91%. For films above 150 nm in thickness, the XRD indicated a partial relaxation of $\varepsilon_\perp$. However for thicknesses up to 400 nm, 100% relaxation was not observed. Fig. 4(b) displays double-axis rocking curves of the Zn_3P_2(008) reflection for 70, 150 and 400 nm thick epilayers. The rocking curve of the 70 nm film was composed of a narrow, coherent scattering peak with FWHM of 16 arcsec, as well as a low-intensity diffuse scattering feature. A diffuse scattering peak is often observed in epitaxial layers and is associated with the presence of point defects [26]. A broadening in the rocking curve was observed for the 150 nm and 400 nm films, with the peak FWHM values increasing to 52 arcsec and 966 arcsec, respectively.

Further evidence of pseudomorphic epilayer growth and strain relaxation was obtained from reciprocal space maps of the GaAs(113) and Zn_3P_2(206) asymmetric reflections that were collected for the 70 nm, 150 nm, and 400 nm thick films (Fig. 5). A relaxation of the in-plane lattice parameter of the Zn_3P_2 epilayer was clearly evident by the comparison of the three measurements. The reciprocal space map of the 70 nm film showed a coherently strained Zn_3P_2 peak with respect to the GaAs substrate. The onset of relaxation was also observed for the 150 nm film, with a noticeable broadening of the film peak.

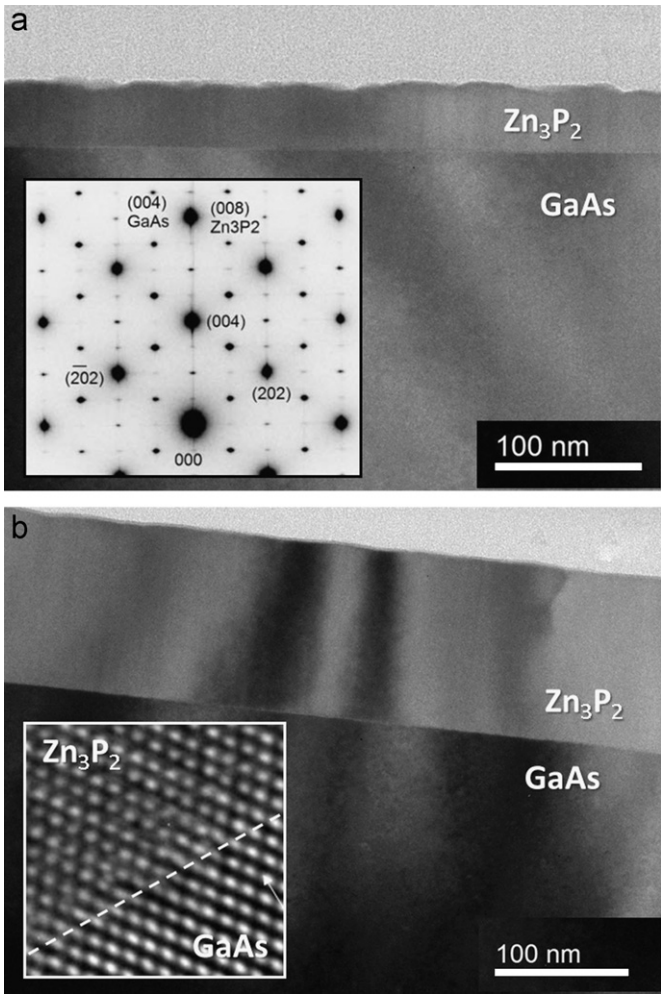

Fig. 3. TEM images of Zn_3P_2 epitaxial layers with thicknesses of (a) 50 nm and (b) 150 nm. The inset in (a) displays a SAED image of the Zn_3P_2/GaAs epitaxial interface. The inset in (b) displays a high-resolution TEM image of the Zn_3P_2/GaAs epitaxial interface.

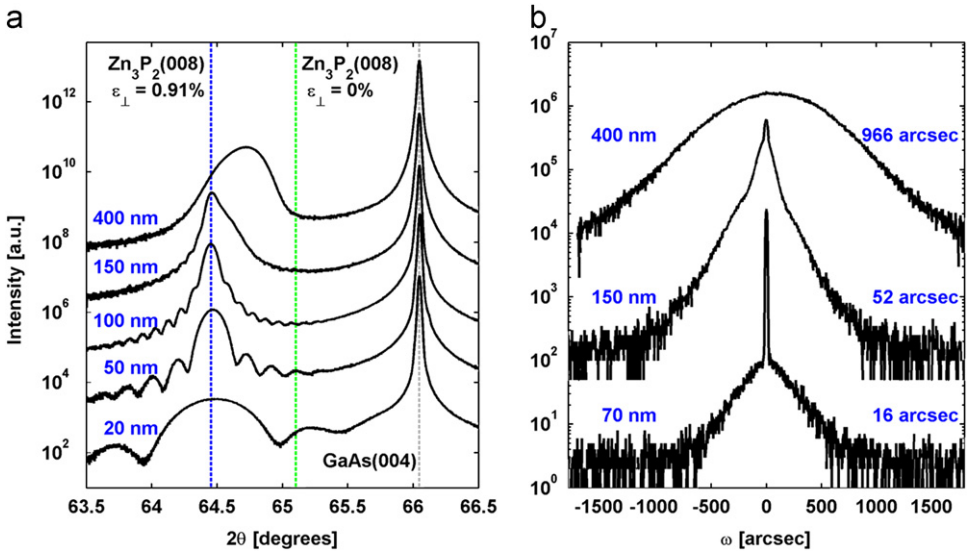

Fig. 4. (a) Symmetric HRXRD scans of the Zn_3P_2(008) and GaAs(004) reflections for increasing Zn_3P_2 layer thickness. Vertical dashed lines represent the Zn_3P_2 peak positions for a fully strained and relaxed unit cell. (b) Rocking curves of the Zn_3P_2(008) reflection for film thicknesses of 70, 150, and 400 nm.

Table 1
Tabulated data for XRD symmetric scans and Van der Pauw and Hall effect measurements.

Thickness [nm]	2θ, Zn_3P_2(008) [deg.]	Partially relaxed?	Resistivity [Ω-cm]	Hole density [cm^{-3}]	Hole mobility [$cm^2 V^{-1} s^{-1}$]
20	64.50(0)	no	1.68 ± 0.06	$3.88 \pm 1.80 \times 10^{17}$	11.0 ± 5.0
50	64.46(3)	no	0.47 ± 0.01	$6.22 \pm 0.70 \times 10^{17}$	21.6 ± 2.7
100	64.45(0)	no	0.27 ± 0.01	$7.94 \pm 0.55 \times 10^{17}$	29.4 ± 2.0
150	64.46(1)	yes	1.06 ± 0.03	$3.12 \pm 0.21 \times 10^{17}$	18.8 ± 1.4
155	64.45(0)	no	2.78 ± 0.06	$5.36 \pm 0.82 \times 10^{16}$	42.6 ± 6.0
170	64.46(1)	yes	18.0 ± 1.2	$2.19 \pm 0.45 \times 10^{16}$	16.4 ± 3.0
275	64.76(2)	yes	60.1 ± 1.8	$1.03 \pm 0.85 \times 10^{16}$	14.8 ± 8.3
400	64.72(2)	yes	3190 ± 46	$8.8 \pm 8.2 \times 10^{14}$	6.2 ± 4.8

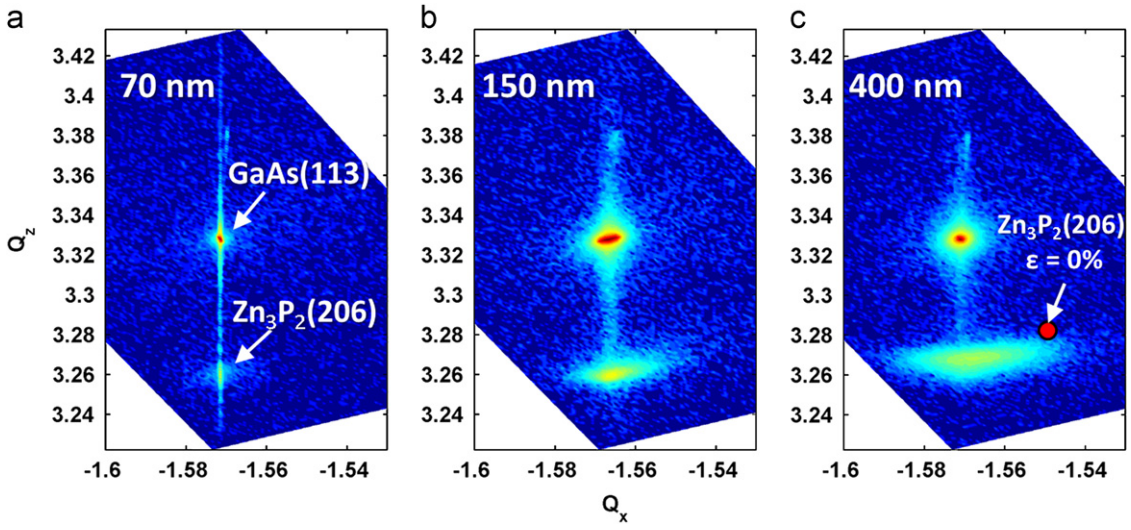

Fig. 5. Reciprocal space maps of the Zn_3P_2(206) and GaAs(113) asymmetric reflections for Zn_3P_2 film thicknesses of (a) 70, (b) 150, and (c) 400 nm. The red dot in (c) represents the position of the fully relaxed Zn_3P_2(206) reflection in reciprocal space. (For interpretation of the references to color in this figure legend, the reader is referred to the web version of this article.)

Finally, the 400 nm film peak was further broadened in the direction of the theoretical position for a fully relaxed film (red dot).

The optical properties of the epitaxial Zn_3P_2 films were determined using spectroscopic ellipsometry. Fig. 6 displays the wavelength dependence of the index of refraction (n) and of the

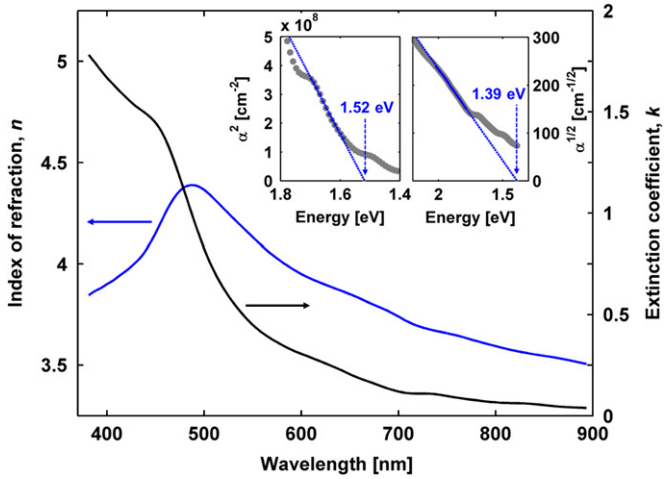

Fig. 6. The index of refraction (n) and extinction coefficient (k) values obtained by spectroscopic ellipsometry on a 7 μm thick Zn_3P_2 film. The insets show the linear extrapolation of α^2 and $\alpha^{1/2}$ as a function of energy, resulting in direct and indirect transition values of 1.52 eV and 1.39 eV.

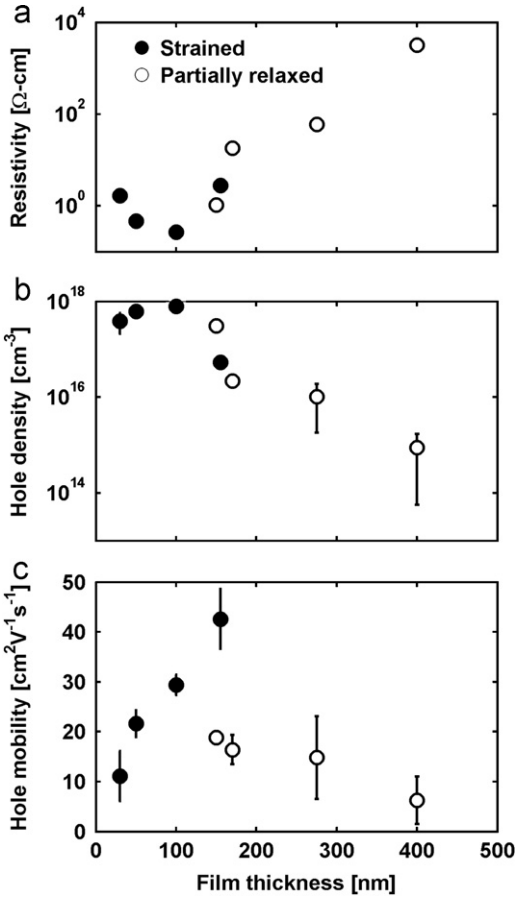

Fig. 7. (a) Van der Pauw resistivity, (b) hole carrier concentration, and (c) hole mobility as a function of Zn_3P_2 epilayer thickness. The filled and open circles represent the data collected on strained and partially relaxed films, respectively.

extinction coefficient (k), as determined on a 7 μm thick Zn_3P_2 film. The measured values of k also allow determination of the energy dependence of the absorption coefficient ($\alpha = 4\pi\lambda/k$) of Zn_3P_2. The insets of Fig. 6 display α^2 and $\alpha^{1/2}$ plotted versus photon energy, near the band edge of Zn_3P_2. Extrapolation of the linear regions of the data yielded values for the direct and indirect band gaps of Zn_3P_2 of 1.52 eV and 1.39 eV, respectively. These values are in excellent agreement with the values previously obtained on bulk Zn_3P_2 wafers [4]. The effect of crystalline relaxation on the optical properties is not well-defined because thin films (<3 μm) of Zn_3P_2 were not fully absorbing near the band edge, which led to interference with the GaAs substrate.

Van der Pauw and Hall effect measurements were performed on 5 mm × 5 mm samples with soldered In contacts. Fig. 7 displays the resistivity, carrier concentration, and Hall mobility of Zn_3P_2 films as a function of epilayer thickness. The electrical measurement results are also tabulated in Table 1. All of the films exhibited p-type conductivity. The resistivity of strained films was consistently on the order of 1 Ω-cm, with corresponding hole concentrations $>1\times10^{17}\,cm^{-3}$. A large increase in resistivity, and consequent decrease in the hole carrier concentration, was observed as the film thickness was increased above 150 nm. The Zn_3P_2 hole mobility also varied as a function of the epilayer thickness. For strained films, an increase in mobility was observed for increasing epilayer thicknesses between 20 and 150 nm. This increase is consistent with a decrease in sensitivity to the interfacial defects between the Zn_3P_2 epilayer and the GaAs substrate. Similar trends have been observed for heteroepitaxial films of InAs on GaAs [27,28], InSb on GaAs [29], and GaN on Al_2O_3 [30]. A maximum hole mobility of $\sim45\,cm^2\,V^{-1}\,s^{-1}$ was observed for a strained 150 nm thick film. This value is comparable to the maximum hole mobility reported for Zn_3P_2 single-crystals that were grown by physical vapor transport [31,32]. Upon partial relaxation of the films, the hole mobility decreased to $<20\,cm^2\,V^{-1}\,s^{-1}$, which is similar to values previously reported for polycrystalline Zn_3P_2 [4].

Theoretical [33] and experimental [31] studies have indicated that the dominant mechanism for intrinsic p-type conductivity in Zn_3P_2 is the production of phosphorus interstitials. This hypothesis agrees well with the observation of diffuse scattering peaks in the HRXRD rocking-curves of the pseudomorphic Zn_3P_2 films. The diffuse scattering is indicative of point defects within the epilayer, and in the case of Zn_3P_2 is consistent with the presence of interstitial phosphorus atoms. A high level of interstitial phosphorus is also consistent with the high concentration of hole carriers observed in strained films by the Hall effect. A subsequent decrease in the hole carrier concentration, and the hole mobility, upon film relaxation is consistent with the occurrence of misfit dislocations and/or threading dislocations within the epilayers. Dislocations have been suggested to act both as charged-carrier scattering and acceptor-compensating regions within a semiconductor material [34]. Therefore, a high density of threading dislocations within a partially relaxed Zn_3P_2 film would be expected to compensate the phosphorus interstitials that are responsible for the intrinsic p-type conductivity, and to thus decrease the effective hole mobility by 50% or more.

4. Conclusions

Tetragonal Zn_3P_2 can be grown epitaxially on GaAs(001) substrates by compound-source molecular-beam epitaxy. Under MBE conditions, the optimal substrate temperature was between 200 °C and 235 °C. The growth window was constrained by amorphous deposition at low temperatures, and at higher temperatures by decreased growth rates and increased surface roughness. TEM and HRXRD studies confirmed that the epitaxial films grew pseudomorphically up to a critical thickness of ~150 nm. Coherent growth allows for further investigations into the effect of strain-related defects on the electronic properties of Zn_3P_2 thin films. Van der Pauw and Hall effect measurements showed that relaxation of the Zn_3P_2 lattice caused a significant decrease in the

effective hole mobility and carrier density. However, below the critical film thickness, p-type mobilities of $>40\ cm^2\ V^{-1}\ s^{-1}$ were observed. These values are comparable to those reported for single-crystal Zn_3P_2. Hence, careful control of strain relaxation will play a key role in the growth of Zn_3P_2 thin films that have optoelectronic properties which are suitable for photovoltaic absorbers.

Acknowledgments

This work was supported by the Dow Chemical Company and by the Department of Energy, Office of Basic Energy Sciences under Grant no. DE-FG02-03ER15483. The authors would like to thank Steve Rozeveld for his assistance with the TEM and SAED measurements. J.P.B. acknowledges support under an NSF graduate research fellowship, and G.M.K. acknowledges support under an NDSEG fellowship.

References

[1] J.M. Pawlikowski, Physical Review B 26 (1982) 4711.
[2] J.M. Pawlikowski, J. Misiewicz, N. Mirowska, Journal of Physics and Chemistry of Solids 40 (1979) 1027–1033.
[3] E. Fagen, Journal of Applied Physics 50 (1979) 6505–6515.
[4] G.M. Kimball, A.M. Müller, N.S. Lewis, H.A. Atwater, Applied Physics Letters 95 (2009) 112103.
[5] N. Wyeth, A. Catalano, Journal of Applied Physics 50 (1979) 1403–1407.
[6] M. Bhushan, A. Catalano, Applied Physics Letters 38 (1981) 39–41.
[7] K.W. Mitchell, Annual Review of Materials Science 12 (1982) 401–413.
[8] M. Bhushan, Applied Physics Letters 40 (1982) 51–53.
[9] T. Suda, K. Kakishita, Journal of Applied Physics 71 (1992) 3039–3041.
[10] T. Suda, K. Kakishita, H. Sato, K. Sasaki, Applied Physics Letters 69 (1996) 2426–2428.
[11] S. Sudhakar, K. Baskar, Journal of Crystal Growth 310 (2008) 2707–2711.
[12] R.C. Schoonmaker, A. Venkitaraman, P.K. Lee, Journal of Physical Chemistry 71 (1967) 2676–2683.
[13] K. Murali, P. Vaya, J. Sobhanadri, Journal of Crystal Growth 73 (1985) 196–198.
[14] S. Fuke, S. Kawarabayashi, K. Kuwahara, T. Imai, Journal of Applied Physics 60 (1986) 2368–2371.
[15] S. Fuke, T. Imai, K. Kawasaki, K. Kuwahara, Journal of Applied Physics 65 (1989) 564–566.
[16] A. Catalano, Journal of Crystal Growth 49 (1980) 681–686.
[17] F.C. Wang, A.L. Fahrenbruch, R.H. Bube, Journal of Electronic Materials 11 (1982) 75–88.
[18] S. Fuke, Y. Takatsuka, K. Kuwahara, T. Imai, Journal of Crystal Growth 87 (1988) 567–570.
[19] C. Rouleau, R. Park, Journal of Applied Physics 73 (1993) 4610–4613.
[20] A. Khatiri, J. Ripalda, T. Krzyzewski, G. Bell, C. McConville, T. Jones, Surface Science 548 (2004) L1–L6.
[21] Y. Ide, M. Yamada, Journal of Vacuum Science and Technology A 12 (1994) 1858–1863.
[22] M. Yamada, Y. Ide, K. Tone, Journal of Applied Physics 31 (1992) L1157–L1160.
[23] Z. Zhu, T. Nomura, M. Miyao, M. Hagino, Journal of Crystal Growth 95 (1989) 529–532.
[24] J.P. Bosco, S.F. Tajdar, H.A. Atwater, Molecular beam epitaxy of n-type ZnS: A wide band gap emitter for heterojunction PV devices, in: Proceedings of the IEEE Photovoltaic Specification Conference, Austin, TX, USA, 2012.
[25] M. von Stackelberg, Zeitschrift für Physikalische Chemie—Abteilung A 28 (1935) 427–460.
[26] M. Birkholz, P.F. Fewster, C. Genzel, Thin film analysis by X-ray scattering, Vch Verlagsgesellschaft Mbh, 2006.
[27] L. Cai, H. Chen, C. Bao, Q. Huang, J. Zhou, Journal of Materials Science 39 (2004) 2637–2640.
[28] S. Kalem, Semiconductor Science and Technology 5 (1990) S200.
[29] T. Zhang, M. Debnath, S. Clowes, W. Branford, A. Bennett, C. Roberts, L. Cohen, R. Stradling, Physica E 20 (2004) 216–219.
[30] W. Fong, C. Zhu, B. Leung, C. Surya, Journal of Crystal Growth 233 (2001) 431–438.
[31] A. Catalano, R. Hall, Journal of Physics and Chemistry of Solids 41 (1980) 635–640.
[32] D. Decroix, V. Muñoz, A. Chevy, Journal of Materials Science 22 (1987) 1265–1270.
[33] S. Demers, A. van de Walle, Physical Review B 85 (2012) 195208.
[34] R. Jaszek, Journal of Materials Science—Materials in Electronics 12 (2001) 1–9.